



Cite this: *Chem. Commun.*, 2021, 57, 8576

Received 10th June 2021,
 Accepted 2nd August 2021

DOI: 10.1039/d1cc03063a

rsc.li/chemcomm

In situ formed Co from a Co–Mg–O solid solution synergizing with LiH for efficient ammonia synthesis†

Wenbo Gao,^a Sheng Feng,^{abc} Hanxue Yan,^{ab} Qianru Wang,^{ab} Hua Xie,^{id a} Ling Jiang,^{id a} Weijin Zhang,^a Yeqin Guan,^{ab} Han Wu,^{ab} Hujun Cao,^{id ab} Jianping Guo^{id *ab} and Ping Chen^{id ab}

A cobalt magnesium oxide solid solution (Co–Mg–O) supported LiH catalyst has been synthesized, in which LiH functions both as a strong reductant for the *in situ* formation of Co metal nanoparticles and a key active component for ammonia synthesis catalysis. Dispersion of the Co–LiH composite on the Co–Mg–O support results in a significantly higher ammonia synthesis rate under mild reaction conditions (19 mmol g⁻¹ h⁻¹ at 300 °C, 10 bar).

Ammonia is the main feedstock of nitrogenous fertilizers for crop growth and is also an attractive energy or hydrogen carrier.¹ Current ammonia manufacture is mainly based on the well-developed Haber–Bosch process, which strongly depends on fossil fuels and accounts for almost 2% of global CO₂ emissions. Thus, the development of a green ammonia synthesis process using renewable energy especially under mild conditions is in demand (*e.g.*, $T < 400$ °C, $P < 5$ MPa).^{2–4} To this end, the development of more efficient catalysts is required. In this regard, it is well known that Ru is more active than Fe under these reaction conditions, and thus recent major research efforts have been devoted to the development of Ru-based catalysts.^{4–8} However, the high price of Ru limits its practical application. As a matter of fact, only a few ammonia synthesis plants have adopted Ru catalysts to date.⁹ It is both of fundamental and practical significance to search for non-Ru catalysts with comparable or even superior performance to Ru to facilitate green ammonia production.

Cobalt is located close to Fe and Ru in the periodic table of elements, and its price is only about 1% of Ru. Although neat Co is less active than Fe or Ru because of its relatively weak N binding energy,¹⁰ its activity can be significantly improved by

alloying it with other transition metals or by the use of effective promoters or functional supports.^{7,11–15} For instance, alloying cobalt and molybdenum resulted in a Co–Mo–N nitride catalyst with activities comparable to those of conventional Ru and Fe catalysts.^{11,12} Hagen reported that BaO was an excellent promoter for cobalt supported on carbon, showing an activity that is close to industrial fused Fe catalysts.¹⁶ Very recently, rare earth metal oxides,¹⁷ N-doped carbon,¹⁸ electrides (*e.g.*, C12A7:e⁻)¹⁵ and oxyhydrides (BaTiO_{2.37}H_{0.63})⁷ were employed as functional supports enhancing the catalytic performance of Co considerably.

Another strategy in activating Co for ammonia synthesis is constructing two-centre catalysts by compositing Co with alkali or alkaline earth metal hydrides.^{19–21} The two-centre catalysts, *e.g.*, Co–LiH and Co–BaH₂, show better activities than that of Cs-promoted Ru catalysts especially at lower temperatures (<350 °C) and have relatively low apparent activation energies and low hydrogen inhibiting effects.^{19,20} These bulk-phase catalysts are usually prepared *via* a ball milling method, however, they suffer from the problems of low specific surface area and limited exposure of active sites. To increase the dispersion of active phases and the potency of hydrides, stable and inert catalyst supports are needed. Given the strong basicity of alkali or alkaline earth metal hydrides, MgO is presumably compatible with these materials. Coincidentally, CoO and MgO are typical rock-salt structures and the metal cations have a similar ionic radius that allows them to easily form a Co–Mg–O solid solution where Co can only partially be reduced from the oxide solution phase.²² Herein, we report that a nano-sized solid solution of Co–Mg–O serves as promising support and Co source for the target Co–LiH catalyst. The *in situ* formed Co metal can synergize with LiH leading to one of the most active Co-based ammonia synthesis catalysts that significantly outperforms the benchmark Cs–Ru/MgO catalyst under mild conditions.

The Co–3Mg–O-co solid solution has a rock-salt structure similar to that of MgO (Fig. 1a). However, the diffraction peaks of the Co–3Mg–O-co sample shift to lower angles by *ca.* 0.2° compared with MgO, indicating the lattice spacing is

^a Dalian National Laboratory for Clean Energy, Dalian Institute of Chemical Physics, Chinese Academy of Sciences, Dalian 116023, China.

E-mail: guojianping@dicp.ac.cn

^b University of Chinese Academy of Sciences, Beijing 100049, China

^c Zhang Dayu School of Chemistry, Dalian University of Technology, Dalian 116024, China

† Electronic supplementary information (ESI) available. See DOI: 10.1039/d1cc03063a

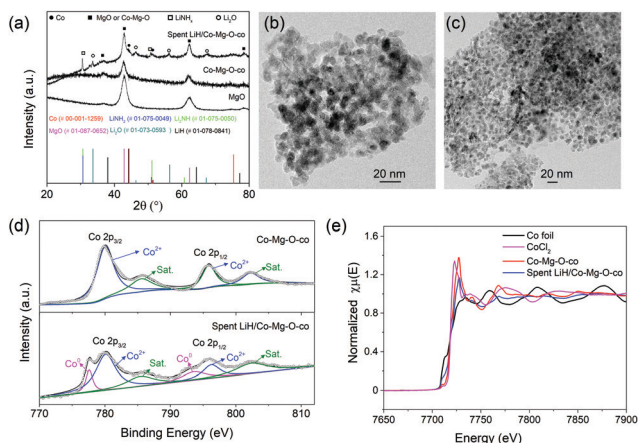


Fig. 1 Characterization of the Co samples. (a) X-Ray diffraction (XRD) patterns of the spent LiH/Co–Mg–O–co catalyst, the Co–Mg–O–co solid solution, and MgO. (b) Transmission electron microscopy (TEM) image of the Co–Mg–O–co solid solution. (c) TEM image of the spent LiH/Co–Mg–O–co catalyst. (d) Co 2p X-ray photoelectron spectroscopy (XPS) profiles of the Co–Mg–O–co solid solution and the spent LiH/Co–Mg–O–co catalyst. (e) X-Ray absorption near edge structure (XANES) spectra of the Co–Mg–O–co solid solution, spent LiH/Co–Mg–O–co catalyst, reference CoCl_2 , and Co foil.

increasing because of the replacement of Mg^{2+} with larger Co^{2+} cations.²³ The TEM image (Fig. 1b) shows that Co–Mg–O–co particles of *ca.* 10 nm pile up. The lattice fringes with distances of 0.25 and 0.21 nm are in agreement with the (111) and (200) lattice spacings of MgO or the Co–Mg–O–co solid solution (Fig. S1, ESI[†]). The chemical state and local environment of Co were measured using XPS and XAS. The signals of $\text{Co}2p_{3/2}$ and $\text{Co}2p_{1/2}$ at 780.1 and 796 eV, and of the satellite at 795.7 and 802.1 eV indicate that cobalt is in the oxidative state (Fig. 1d), which agrees well with the results of XANES (Fig. 1e) characterizations. The specific surface area of the Co–3Mg–O–co sample reached $250 \text{ m}^2 \text{ g}^{-1}$ and was examined as a support and Co source for the Co–LiH catalyst.

The Co–Mg–O supported LiH sample, *e.g.*, 5LiH/Co–3Mg–O–co was prepared *via* the impregnation method using liquid ammonia as the solvent as shown in the experimental section. The sample was evaluated as a catalyst in ammonia synthesis and collected after the catalytic test for further characterizations. The loadings of Co and Li were determined to be 21.3 wt% and 17.1 wt% using ICP-AES, respectively. The morphology and textural structure of the LiH/Co–Mg–O catalyst was studied. The TEM image shows that the morphology of the sample is maintained after the catalytic test (Fig. 1c). STEM-EDX mapping images for the fresh and spent catalysts show overlapping of the elements Co and Mg, suggesting the existence of a Co–Mg–O solid solution (Fig. S2, ESI[†]). The nitrogen adsorption–desorption isotherms show the presence of a macroporous structure in the fresh and spent samples (Fig. S3, ESI[†]). The XRD pattern of the spent sample shows weak peaks at around 44.3° , 51.5° , and 75.1° , which are ascribed to cubic Co metal nanoparticles (Fig. 1a). However, it is difficult to determine the particle size of Co from the TEM image (Fig. 1c). It has been reported that metallic Co can only

be formed by reducing Co–Mg–O solid solutions above 700°C in a flow of H_2 , which is due to the strong interaction of CoO with the MgO matrix.²⁴ The metallic Co in the 5LiH/Co–3Mg–O–co sample is likely formed *in situ via* the redox reaction between LiH and the Co–Mg–O solid solution at a much lower temperature (*ca.* 300°C). This is partly supported by the formation of the Li_2O phase (Fig. 1a). The chemical state and local environment of Co in the used catalyst were further characterized using XPS and XAS. As shown in Fig. 1d, the appearance of signals at 777.6 and 793.5 eV evidence that part of the Co^{2+} is reduced to the metallic state. The molar ratio of surface $\text{Co}^{2+}/\text{Co}^0$ is estimated to be 2.6 : 1, showing that nearly 28% of the (sub)surface Co atoms are in their metallic state. XANES characterization results also show that part of the Co^{2+} is reduced to Co^0 (Fig. 1e). The appearance of LiNH_2 and/or Li_2NH was verified by both the XRD pattern (Fig. 1a) and the absorption bands at around 3313, 3258, and 3183 cm^{-1} ,^{25,26} respectively in the IR spectrum (Fig. S4, ESI[†]). The specific surface area of the used sample is $96 \text{ m}^2 \text{ g}^{-1}$, which is more than twice that of the Co–LiH catalyst ($42 \text{ m}^2 \text{ g}^{-1}$). Due to the higher specific surface area, it is expected that the supported Co–LiH would expose more reactive sites and thus be more active than Co–LiH for ammonia synthesis.

To test the effect of the Co–Mg–O support, optimization of the Co/Mg molar ratio was first explored and an activity maximum was found on the LiH/Co–3Mg–O–co sample with a Co/Mg molar ratio of 1/3 (Fig. S5a, ESI[†]). In addition, different Co–Mg–O supports prepared using deposition–precipitation and impregnation methods were also used for loading LiH and tested for ammonia synthesis. A comparison of the catalytic activities of the three catalysts is shown in Fig. S6a (ESI[†]). It is seen that the LiH/Co–Mg–O–co shows the best catalytic performance in the temperature range of 200 to 350°C and 10 bars. Fig. 2a shows the mass-based activities of LiH/Co–Mg–O–co, Co–Mg–O–co, and Co–LiH samples for the ammonia synthesis reaction. The molar ratio of LiH to Co is 5 : 1 for both LiH-containing samples. The pristine Co–Mg–O–co solid solution shows negligible activity for ammonia synthesis below 350°C . While the LiH/Co–Mg–O–co catalyst shows much more enhanced activities than both Co–LiH and Co–Mg–O–co for temperatures ranging from 200 to 350°C . The ammonia synthesis rate of LiH/Co–Mg–O–co reaches 1.5, 19.0, and $39.8 \text{ mmol g}^{-1} \text{ h}^{-1}$ at 200, 300, and 350°C , respectively, which is *ca.* 3.5–4 times of that of the Co–LiH catalyst. As a comparison, a Li_2O -promoted Co/MgO catalyst (denoted $\text{Li}_2\text{O-Co/MgO}$) was synthesized and tested. Its activity is only $12.8 \mu\text{mol g}^{-1} \text{ h}^{-1}$ at 400°C (Fig. S7, ESI[†]), indicating Li_2O is not an efficient promoter for the Co catalyst.

Fig. 2b and Table S1 (ESI[†]) compare the activities of various Co- and Ru-based catalysts. It can be seen that LiH/Co–Mg–O–co is among the most active ammonia synthesis catalysts. In particular, LiH/Co–Mg–O–co has an ammonia synthesis rate of $19 \text{ mmol g}^{-1} \text{ h}^{-1}$ at 300°C , which is 4 times that of the $\text{BaH}_2\text{-Co/CNTs}$ catalyst (*ca.* $4.8 \text{ mmol g}^{-1} \text{ h}^{-1}$). Although it has a higher WHSV and was used at a lower temperature, the NH_3 yield of LiH/Co–Mg–O–co at 350°C (3.25%) is *ca.* 3.1 and 14.8 times of that of the Co/C12A7:e⁻¹⁵ and Co/BaTiO_{2.37}H_{0.63}⁷

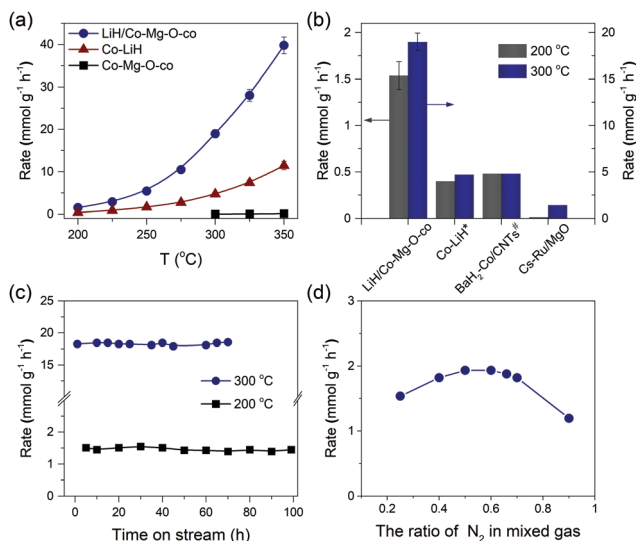


Fig. 2 Catalytic performance of the LiH/Co-Mg-O-co and reference catalysts. (a) Temperature dependence of NH₃ synthesis rate of various Co-based catalysts at 10 bar of syngas (N₂:H₂ = 1:3) and a weight hourly space velocity (WHSV) of 60 000 mL g⁻¹ h⁻¹. (b) Activities of the LiH/Co-Mg-O-co catalyst and some reference Co and Ru-based catalysts at 200 and 300 °C, respectively. * and #, the ammonia synthesis rates were taken from ref. 19 and 20, respectively. (c) Time dependence of the catalytic activities of the LiH/Co-Mg-O-co catalyst at 200 °C and 300 °C, 10 bar, respectively. (d) Ammonia synthesis rate as a function of the ratio of N₂ in a mixed gas over the LiH/Co-Mg-O-co catalyst. Reaction conditions: 200 °C, 10 bar, WHSV = 60 000 mL g⁻¹ h⁻¹. Error bars in (a and b) represent the standard deviation from three independent measurements.

catalysts at 400 °C, respectively. Moreover, the ammonia synthesis rate of LiH/Co-Mg-O-co at 300 °C and 10 bar is more than one order of magnitude higher than that of the highly active Cs-Ru/MgO and surpasses most recently reported Ru-based catalysts under similar reaction conditions (Table S1, ESI†). The stability test shows that the activity remains constant at 200 °C or 300 °C and 10 bar (Fig. 2c). The molar ratio of N₂/H₂ also influences the performance of the catalyst. As shown in Fig. 2d, the optimal ratio is found at around 1:1 and 3:2 showing a higher N₂ partial pressure is preferable. It is worth noting that the fluctuation of activity is only 20% when the N₂/H₂ ratio varies from 1:3 to 7:3 showing that this catalyst can tolerate the change of N₂/H₂ molar ratio over a relatively wide range. These features are important for its compatibility with renewable energy storage and utilization.

Fig. S8a and Table S2 (ESI†) show the apparent activation energies (E_a) of a series of Co catalysts for ammonia synthesis. The E_a of LiH/Co-Mg-O-co is 55.8 ± 2.2 kJ mol⁻¹ in the temperature range of 200 to 300 °C, which is similar to those of Co-LiH, LiH/Co-Mg-O-p and LiH/Co-Mg-O-i (i.e., 52–59 kJ mol⁻¹, see Table S2 and Fig. S5b, S6b, ESI†). These results suggest that the dispersion of LiH on the Co-Mg-O support creates the same type of active site as the Co-LiH composite catalyst and the activity enhancement could be explained by the increasing number of active sites on the catalyst.²⁷

Kinetic studies show that the reaction order with respect to N₂ is 0.76 (Fig. S7b, ESI†), which is close to 1 and consistent

with most of the conventional ammonia synthesis catalysts.^{16,28} Some recent reports showed that the reaction order of N₂ is ca. 0.5,^{6,19,29} which has been considered to be an indication that the dissociative chemisorption of N₂ is no longer the rate-determining step (RDS). It should be noted that the measurement of the N₂ reaction order should be done under constant partial pressures of H₂ and NH₃ (see the ESI†). Although the ammonia partial pressure is pretty low, it has a substantial effect on the N₂ and H₂ reaction orders. Therefore, we suggest the N₂ and H₂ reaction orders should be measured under a constant ammonia partial pressure. A typical example showing the dramatic effect of ammonia partial pressure on the reaction orders of N₂ and H₂ can be found in Table S2 (ESI†). The reaction order with respect to H₂ for the LiH/Co-Mg-O-co is 1.19 (Fig. S7c, ESI†), in clear contrast to the reported Co/C catalyst that has a negative H₂ reaction order (−0.4 at 400 °C).¹⁶ The NH₃ reaction order is correspondingly negative (−0.94) for the LiH/Co-Mg-O-co catalyst (Fig. S7d, ESI†), indicating the inhibiting effect of NH₃.

It has been reported that LiH is able to fix N₂ to form Li₂NH and H₂.³⁰ Here a redox reaction between LiH and N₂ takes place, where N₂ is reduced and the H⁻ in LiH is oxidized to H⁺ and H₂. Therefore, the formation of H₂ during a N₂-TPR-MS measurement is an indication of N₂ activation on the hydride (H⁻)-containing samples. The presence of Co can catalyze this reaction as clearly seen in Fig. 3, shifting the temperature for H₂ release downwards by 43 °C. As inferred from the kinetic studies and N₂-TPR results, we assumed that the activation of N₂ occurred at the interface of the Co metal and LiH. Our previous work showed that ternary metal hydride species could function as the active site for N₂ activation and hydrogenation.³¹ To reveal the interaction of Co and LiH, we resorted to gas-phase cluster measurements.^{31,32} As shown in Fig. S7 (ESI†), the peaks in the mass spectrum of the gas-phase clusters bombarded by the Co-LiH sample could be assigned to a series of [Li-Co-H] clusters such as [Li₄CoH₄]⁻, [Li₆CoH₆]⁻ and [Li₇CoH₈]⁻, etc. Theoretical calculations also showed that bulk LiCoH₃ has moderate thermodynamic stability.³³ Although the local composition and structure of surface species on the LiH/Co-Mg-O catalyst may not be the same as these gas-phase cluster species, the formation of [Li-Co-H] clusters suggests a

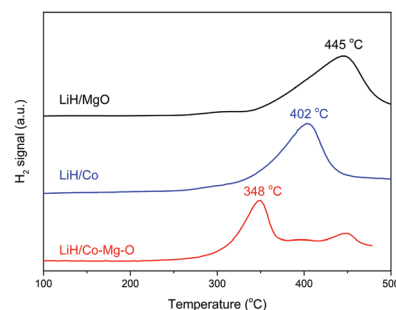


Fig. 3 Temperature-programmed reaction (N₂-TPR-MS) profiles of a series of LiH-containing samples in a N₂ flow. The formation of H₂ indicates the redox reaction of N₂ and LiH. Reaction conditions: 1 bar of N₂, ramping rate of 5 °C min⁻¹.

strong and synergistic interaction between LiH and Co, which provides valuable insight for further studies. It could be expected that the close contact and intrinsic interaction of Co and LiH is vitally important to the catalysis. When dispersed on the surface of the Co–Mg–O support, some LiH may be used to reduce Co–Mg–O to Co metal *in situ*. The newly formed Co metal may have a better chance of interaction with LiH nearby creating more reactive sites for N₂ conversion and hydrogenation to NH₃. As shown in Fig. 3, the H₂-release of LiH/Co–Mg–O starts at *ca.* 200 °C and the peak temperature is lowered to *ca.* 350 °C, which is 50 °C lower than that of LiH/Co, demonstrating that the N₂ activation and hydrogenation is more favourable on the supported LiH/Co–Mg–O sample. The smaller Co particle size and more contact between Co and LiH should account for this phenomenon. The formation of Li₂NH species was verified from the FTIR spectrum (Fig. S3, ESI†).

In summary, a Co–Mg–O solid solution has been demonstrated as an efficient support and Co source for loading LiH in ammonia synthesis. LiH functions both as a strong reductant for the formation of metallic Co *in situ* from the Co–Mg–O solid solution and is a key component when synergizing with Co, enabling a highly active and stable catalyst for ammonia synthesis. The dispersion of Co–LiH on the Co–Mg–O support resulted in one of the highest ammonia synthesis rates and NH₃ yields among Co-based catalysts for ammonia synthesis (19 mmol_{NH₃} g⁻¹ h⁻¹ and 1.55% at 300 °C, 10 bar, respectively), which considerably outperforms the benchmark Cs–Ru/MgO catalyst. This shows the potential for cobalt-based catalysts to be coupled in renewable energy-driven ammonia synthesis. With the development of more active and stable Co-based catalysts, this “green” ammonia production process could be energy- and cost-competitive towards the existing fossil fuel-dependent Haber–Bosch process.

This work is in celebration of the 10th Anniversary of the Founding of the Youth Innovation Promotion Association of the Chinese Academy of Sciences. The authors are grateful for the financial support from the National Natural Science Foundation of China (Grant No. 21922205, 21872137, 21633011, 21988101, 51801197), the Youth Innovation Promotion Association CAS (No. 2018213, 2019189), and the K. C. Wong Education Foundation (GJTD-2018-06). The authors are also grateful to the Shanghai Synchrotron Radiation Facility for providing the beam time.

Conflicts of interest

There are no conflicts to declare.

Notes and references

- 1 J. Guo and P. Chen, *Chemistry*, 2017, **3**, 709–712.
- 2 J. G. Chen, R. M. Crooks, L. C. Seefeldt, K. L. Bren, R. M. Bullock, M. Y. Darensbourg, P. L. Holland, B. Hoffman, M. J. Janik, A. K. Jones,

- M. G. Kanatzidis, P. King, K. M. Lancaster, S. V. Lymar, P. Pfromm, W. F. Schneider and R. R. Schrock, *Science*, 2018, **360**, eaar6611.
- 3 J. Norskov and J. G. Chen, US DoE Round Table Report, 2016.
- 4 J. W. Zheng, F. L. Liao, S. Wu, G. Jones, T. Y. Chen, J. Fellowes, T. Sudmeier, I. J. McPherson, I. Wilkinson and S. C. E. Tsang, *Angew. Chem., Int. Ed.*, 2019, **58**, 17335–17341.
- 5 H. Bielawa, O. Hinrichsen, A. Birkner and M. Muhler, *Angew. Chem., Int. Ed.*, 2001, **40**, 1061.
- 6 M. Kitano, Y. Inoue, Y. Yamazaki, F. Hayashi, S. Kanbara, S. Matsuishi, T. Yokoyama, S.-W. Kim, M. Hara and H. Hosono, *Nat. Chem.*, 2012, **4**, 934–940.
- 7 Y. Tang, Y. Kobayashi, N. Masuda, Y. Uchida, H. Okamoto, T. Kageyama, S. Hosokawa, F. Loyer, K. Mitsuhara, K. Yamanaka, Y. Tamenori, C. Tassel, T. Yamamoto, T. Tanaka and H. Kageyama, *Adv. Energy Mater.*, 2018, **8**, 1801772.
- 8 Y. Ogura, K. Sato, S. I. Miyahara, Y. Kawano, T. Toriyama, T. Yamamoto, S. Matsumura, S. Hosokawa and K. Nagaoka, *Chem. Sci.*, 2018, **9**, 2230–2237.
- 9 H. Z. Liu, *Chin. J. Catal.*, 2014, **35**, 1619.
- 10 A. Vojvodic, A. J. Medford, F. Studt, F. Abild-Pedersen, T. S. Khan, T. Bligaard and J. K. Norskov, *Chem. Phys. Lett.*, 2014, **598**, 108–112.
- 11 C. J. Jacobsen, S. Dahl, B. S. Clausen, S. Bahn, A. Logadottir and J. K. Norskov, *J. Am. Chem. Soc.*, 2001, **123**, 8404–8405.
- 12 R. Kojima and K. Aika, *Appl. Catal., A*, 2001, **218**, 121.
- 13 S. Hagen, R. Barfod, R. Fehrmann, C. J. Jacobsen, H. T. Teunissen, C. Stahl and I. Chorkendorff, *Chem. Commun.*, 2002, 1206–1207.
- 14 D. McKay, D. H. Gregory, J. S. J. Hargreaves, S. M. Hunter and X. Sun, *Chem. Commun.*, 2007, 3051–3053.
- 15 Y. Inoue, M. Kitano, M. Tokunari, T. Taniguchi, K. Ooya, H. Abe, Y. Niwa, M. Sasase, M. Hara and H. Hosono, *ACS Catal.*, 2019, **9**, 1670–1679.
- 16 S. Hagen, R. Barfod, R. Fehrmann, C. J. H. Jacobsen, H. T. Teunissen and I. Chorkendorff, *J. Catal.*, 2003, **214**, 327–335.
- 17 B. Y. Lin, Y. C. Qi, K. M. Wei and J. X. Lin, *RSC Adv.*, 2014, **4**, 38093–38102.
- 18 X. Wang, X. Peng, W. Chen, G. Liu, A. Zheng, L. Zheng, J. Ni, C. T. Au and L. Jiang, *Nat. Commun.*, 2020, **11**, 653.
- 19 P. Wang, F. Chang, W. Gao, J. Guo, G. Wu, T. He and P. Chen, *Nat. Chem.*, 2017, **9**, 64–70.
- 20 W. B. Gao, P. K. Wang, J. P. Guo, F. Chang, T. He, Q. R. Wang, G. T. Wu and P. Chen, *ACS Catal.*, 2017, **7**, 3654–3661.
- 21 W. B. Gao, J. P. Guo and P. Chen, *Chin. J. Chem.*, 2019, **37**, 442–451.
- 22 L. Wang, A. Navrotsky, R. Stevens, B. F. Woodfield and J. Boerio-Goates, *J. Chem. Thermodyn.*, 2003, **35**, 1151–1159.
- 23 X. Guo, Y. Li, R. Shi, Q. Liu, E. Zhan and W. Shen, *Appl. Catal., A*, 2009, **371**, 108.
- 24 A. A. Vedyagin, T. M. Karnaukhov, S. V. Cherepanova, V. O. Stoyanovskii, V. A. Rogov and I. V. Mishakov, *Int. J. Hydrogen Energy*, 2019, **44**, 20690–20699.
- 25 Y. Kojima and Y. Kawai, *J. Alloys Compd.*, 2005, **395**, 236–239.
- 26 P. Chen, Z. Xiong, J. Luo, J. Lin and K. L. Tan, *J. Phys. Chem. B*, 2003, **107**, 10967.
- 27 X. Xie, Y. Li, Z.-Q. Liu, M. Haruta and W. Shen, *Nature*, 2009, **458**, 746.
- 28 F. Rosowski, A. Hornung, O. Hinrichsen, D. Herein, M. Muhler and G. Ertl, *Appl. Catal., A*, 1997, **151**, 443–460.
- 29 Y. Kobayashi, Y. Tang, T. Kageyama, H. Yamashita, N. Masuda, S. Hosokawa and H. Kageyama, *J. Am. Chem. Soc.*, 2017, **139**, 18240–18246.
- 30 W. Gao, J. Guo, P. Wang, Q. Wang, F. Chang, Q. Pei, W. Zhang, L. Liu and P. Chen, *Nat. Energy*, 2018, **3**, 1067–1075.
- 31 P. K. Wang, H. Xie, J. P. Guo, Z. Zhao, X. T. Kong, W. B. Gao, F. Chang, T. He, G. T. Wu, M. S. Chen, L. Jiang and P. Chen, *Angew. Chem., Int. Ed.*, 2017, **56**, 8716–8720.
- 32 C. Cui, Y. Jia, H. Zhang, L. Geng and Z. Luo, *J. Phys. Chem. Lett.*, 2020, **11**, 8222–8230.
- 33 S. Takagi, H. Saitoh, N. Endo, R. Sato, T. Ikeshoji, M. Matsuo, K. Miwa, K. Aoki and S.-I. Orimo, *Phys. Rev. B: Condens. Matter Mater. Phys.*, 2013, **87**, 125134.